Geophysical Journal International

Geophys. J. Int. (2016) **206,** 1539–1551
Advance Access publication 2016 July 8
GJI Seismology

doi: 10.1093/gji/ggw228

Two-dimensional time-domain finite-difference modeling for viscoelastic seismic wave propagation

Na Fan,[1] Lian-Feng Zhao,[1] Xiao-Bi Xie,[2] Zengxi Ge[3] and Zhen-Xing Yao[1]

[1] *Key Laboratory of Earth and Planetary Physics, Institute of Geology and Geophysics, Chinese Academy of Sciences, Beijing* 100029, *China.*
E-mail: zhaolf@mail.igcas.ac.cn
[2] *Institute of Geophysics and Planetary Physics, University of California at Santa Cruz, CA* 95064, *USA*
[3] *School of Earth and Space Sciences, Peking University, Beijing* 100871, *China*

Accepted 2016 June 13. Received 2016 June 9; in original form 2015 September 19

SUMMARY

Real Earth media are not perfectly elastic. Instead, they attenuate propagating mechanical waves. This anelastic phenomenon in wave propagation can be modeled by a viscoelastic mechanical model consisting of several standard linear solids. Using this viscoelastic model, we approximate a constant Q over a frequency band of interest. We use a four-element viscoelastic model with a trade-off between accuracy and computational costs to incorporate Q into 2-D time-domain first-order velocity–stress wave equations. To improve the computational efficiency, we limit the Q in the model to a list of discrete values between 2 and 1000. The related stress and strain relaxation times that characterize the viscoelastic model are pre-calculated and stored in a database for use by the finite-difference calculation. A viscoelastic finite-difference scheme that is second order in time and fourth order in space is developed based on the MacCormack algorithm. The new method is validated by comparing the numerical result with analytical solutions that are calculated using the generalized reflection/transmission coefficient method. The synthetic seismograms exhibit greater than 95 per cent consistency in a two-layer viscoelastic model. The dispersion generated from the simulation is consistent with the Kolsky–Futterman dispersion relationship.

Key words: Numerical solutions; Elasticity and anelasticity; Seismic attenuation; Wave propagation.

1 INTRODUCTION

The materials that compose the Earth are not perfectly elastic. When seismic waves propagate within the Earth, both attenuation and waveform distortion can be observed. Under these circumstances, the anelasticity of the Earth often cannot be neglected in seismic modeling and data processing (Samec & Blangy 1992; Wang 2009).

The attenuation property is commonly characterized by a dimensionless quality factor Q, which is defined in terms of the mean energy stored in the medium divided by the energy lost during a single cycle. Over the past three decades, extensive efforts have sought to develop modeling methods for wave propagation in viscoelastic media. These approaches can be grouped into two categories. Methods in the first category use the fractional time derivative to obtain the convolution stress–strain relationship which forms the constant-Q model given by Kjartansson (1979), (Carcione *et al.* 2002; Carcione 2008). The fractional time derivative is transformed into a fractional Laplacian operator (Chen & Holm 2004) and calculated using the fractional Fourier pseudospectral method. This technique avoids storing wavefield, and thus, the modeling is as efficient as in lossless media (Carcione 2010; Treeby & Cox 2010; Zhu & Carcione 2014; Zhu & Harris 2014). Methods in the second category use a spectrum of relaxation mechanisms to describe the viscoelastic constitutive relationship (Emmerich & Korn 1987; Robertsson *et al.* 1994; Day & Bradley 2001). The generalized standard linear solid (GSLS, also called the generalized Zener body or GZB by some authors) and generalized Maxwell body (GMB) are widely used as viscoelastic models to introduce the memory variables into propagation modeling (Robertsson *et al.* 1994; Kristek & Moczo 2003). With this technique, the viscoelastic wave equation can easily be solved using a time-marching scheme, such as the finite-difference, finite-element or pseudospectral methods. Day & Minster (1984) were the first to propose a framework for incorporating the convolution operator into the time-marching algorithm to compute theoretical seismograms. Their approach uses the Padé approximant to transform the convolution integral, which relates stress to strain history, into a convergent sequence of constant-coefficient differential operators of increasing order. Emmerich & Korn (1987) improved the accuracy and efficiency of this approach by considering the rheology model of GMB, in which the viscoelastic moduli have the desired rational form. Carcione *et al.* (1988a,b,c) developed an alternative approach based on the rheology of GSLS.

Two parallel sets of formulations were developed. The GMB approach introduced anelastic functions into the wave equation. This technique was subsequently refined by others (Krebes & Quiroga-Goode 1994; Kristek & Moczo 2003). The GSLS approach incorporated memory variables into the wave equation and this method was further developed for the 2-D and 3-D displacement–stress or velocity–stress formulations of both viscoacoustic and viscoelastic wave equations (Tal-Ezer *et al*. 1990; Carcione 1993; Robertsson *et al*. 1994; Blanch *et al*. 1995; Xu & McMechan 1995). Although the constitutive relationships of GZB and GMB differ, the two resulting viscoelastic models are essentially the same (Moczo & Kristek 2005; Cao & Yin 2014).

Robertsson *et al*. (1994) used a fourth-order spatial and second-order temporal staggered finite-difference scheme to solve the first-order velocity–stress viscoelastic wave equation using the GSLS model in 2-D and 3-D media. Because of its simplicity and high efficiency, this method has been widely extended to other applications, such as viscoelastic modeling that includes surface topography (Robertsson 1996; Hestholm 1999; Hestholm & Ruud 2000), parallel 3-D viscoelastic modeling (Bohlen 2002), rotated staggered-grid modeling (Saenger & Bohlen 2004) and spectral-element modeling (Komatitsch & Tromp 1999). In this study, we improved the expressions of memory variables by separating the memory variables of *P* and *S* waves based on the method of Robertsson *et al*. (1994) and implemented 2-D viscoelastic finite-difference modeling. Based on a constant Q model over a specified frequency band, we construct a database composed of several stress and strain relaxation times corresponding to different Q values. The viscoelastic database can be directly called by the finite-difference program, which greatly reduces the modeling calculation. To validate our approach, we calculate the 2-D viscoelastic finite-difference modeling in benchmark models and compare numerical results with analytical seismograms calculated using the generalized reflection/transmission coefficient method (GRTM). These numerical results reveal that our method can accurately reproduce the amplitude decay and waveform dispersion caused by anelastic attenuation.

2 VISCOELASTIC MODEL

Linear viscoelastic theory is based on the Boltzmann superposition principle and is applicable for small deformations. The current status of the stress in the model is determined by the superposition of responses at previous times, and the material is considered to have a memory because the current stress depends on the full strain history (Christensen 1982). The viscoelastic constitutive relationship between stress and strain is described as

$$\sigma(t) = G(t) * \dot{\varepsilon}(t) = \dot{G}(t) * \varepsilon(t), \tag{1}$$

where $*$ denotes the time convolution, $\varepsilon(t)$ is the strain, $\sigma(t)$ is the stress and $G(t)$ is the relaxation function. A dot above a variable indicates a time derivative.

Liu *et al*. (1976) demonstrated that a GSLS model composed of multiple relaxation mechanisms can explain attenuation observed both in the Earth and in laboratory experiments. The relaxation function $G(t)$ of a GSLS composed of multiple parallel SLSs can be expressed by summing the parameters of the individual SLSs:

$$G(t) = M_R\left(1 - \sum_{l=1}^{L}\left(1 - \frac{\tau_{\varepsilon l}}{\tau_{\sigma l}}\right)e^{-t/\tau_{\sigma l}}\right)\theta(t), \tag{2}$$

where M_R is the relaxed modulus, L is the number of SLSs in the viscoelastic model, $\tau_{\sigma l}$ and $\tau_{\varepsilon l}$ are the stress and strain relaxation times of the lth SLS and $\theta(t)$ is the Heaviside function.

2.1 Incorporating the Q model into the viscoelastic wave equation

The quality factor Q, which quantifies the attenuation property of a medium, should be incorporated into the wave equation and solved by time-domain numerical methods. By applying Fourier transform to the time derivative of the relaxation function (2), we obtain the complex modulus of the viscoelastic model

$$M(\omega) = F\left[\dot{G}(t)\right], \tag{3}$$

where ω is the angular frequency and F denotes the Fourier transform.

The complex modulus $M(\omega)$ represents the linear relationship between the stress and strain in the frequency domain. The relationship between Q and the complex modulus of the viscoelastic model can be described as follows (O'connell & Budiansky 1978):

$$Q(\omega) = \frac{\mathrm{Re}\left[M(\omega)\right]}{\mathrm{Im}\left[M(\omega)\right]}, \tag{4}$$

where Re and Im are the real and imaginary parts of $M(\omega)$, respectively.

From eq. (2) to (4), the frequency-domain relationship between Q and the viscoelastic parameters in a GSLS model can be obtained as follows (Blanch *et al*. 1995):

$$Q(\omega) = \frac{1 - L + \sum_{l=1}^{L}\frac{1+\omega^2\tau_{\varepsilon l}\tau_{\sigma l}}{1+\omega^2{\tau_{\sigma l}}^2}}{\sum_{l=1}^{L}\frac{\omega(\tau_{\varepsilon l}-\tau_{\sigma l})}{1+\omega^2{\tau_{\sigma l}}^2}}. \tag{5}$$

Several techniques have been proposed to obtained relaxation times in eq. (5) for a given $Q(\omega)$. For example, Blanch *et al*. (1995) suggested the τ-method, and Liu & Archuleta (2006) proposed the empirical interpolation method. These techniques were simple but often sacrificed certain accuracies. In this study, we develop an alternative method by adopting a formal inversion to determine relaxation times from Q. An inversion method is usually very time consuming, particularly if needs to calculate for every gridpoint. To mitigate this difficulty, we convert continues Q value into a discretized Q within the commonly used range of $Q = 2$–1000. In this way, we only need to inverse approximately 1000 Q values. This procedure is moved out from the finite-difference code. After determine the optimal number of SLSs and obtain relaxation times for a frequency-dependent Q model, we create a database, in which tabulated Q values are linked to multiple relaxation times. Before calculation, the finite-difference code will visit the database and read the relaxation times. If large number of finite differences need be calculated, such as in an iterative process in the full-waveform inversion, the database can be used repeatedly.

Frequency band-limited constant *P*- and *S*-wave Q models are widely accepted in earthquake seismology (Kjartansson 1979; Spencer 1981; Murphy 1982), and their attenuation–dispersion relationships have been extensively investigated (Futterman 1962). Thus, we use a spectrum of viscoelastic parameters to simulate the constant Q model. The frequency range we consider is between 0.05 and 25.0 Hz, within which seismic waves from natural earthquakes

are observable. To optimize the model parameters, we adopt an objective function

$$E = \sqrt{\frac{1}{N-1}\sum_{n=1}^{N}[Q(\omega_n) - Q_{\text{cst}}]^2}, \tag{6}$$

where ω_n are the discrete frequencies used to check the Q model, N is the number of frequencies log-evenly distributed in the frequency band of interest, $Q(\omega_n)$ is from eq. (4) and is calculated using eq. (5) and Q_{cst} is a constant Q within the frequency band. Minimizing this objective function can determine the viscoelastic parameters in eq. (5).

We attempt to obtain the desired constant-Q behaviour while reducing computational costs to solve viscoelastic equations, particularly if the problem is 3-D, because the number of memory variable equations (see the viscoelastic wave equation in Section 3) is proportional to L and involves extra computational costs to solve the wave equations. We first determine the optimal number of SLSs in eq. (5) and then use an inversion method to determine the stress and strain relaxation times for each SLS. We test the viscoelastic models with different numbers of SLSs to construct the parameter database. The viscoelastic parameters are obtained using the simulated annealing method (Szu & Hartley 1987; Ingber 1989). Given that $Q = 100$, the viscoelastic parameters in the $L = 2$–10 SLSs models can be inverted. Fig. 1 presents the (a) standard deviations, (b) relative errors and (c) approximation curves for a constant Q model. The approximation error becomes smaller as L increases, but the simulation calculation cost may also increase due to the increasing number of memory variable equations. Considering the trade-off between the approximation error and computational costs, we choose $L = 4$ to construct a reasonable viscoelastic model. Note that, the number of elements is related to the bandwidth of the Q model. Given an accuracy, a wideband Q model usually requires more SLSs, and a narrowband Q needs less SLSs. After L is determined, the stress and strain relaxation times that correspond to integer Q values over the commonly used range of 2–1000 are inverted and stored as the viscoelastic-parameter database, which can be called later by the finite-difference program.

In Liu & Archuleta (2006) approach, they set the minimum and maximum Q as 5 and 5000, the number of relaxation mechanisms $L = 8$, and the frequency band 0.01–50 Hz. They first determine the viscoelastic parameters for minimum and maximum Q, followed by using interpolation to obtain parameters for intermediate Q values. The empirical interpolation formula obtained from numerical calculation cannot be easily extended to cases with different frequency dependency or different number of relaxation mechanisms. In order to compare the accuracy between two approaches, we apply our method to their case and the results are shown in Fig. 2, where (a)–(d) are for $Q = 10$, 100, 1000 and 5000. The red and blue lines are for ours and Liu's results. In general, our approach generates smaller errors in the entire frequency band, especially for lower Q cases.

2.2 Dispersion relationship

According to eq. (2), the relaxation function is related to the relaxed modulus and relaxation times. We have obtained L pairs of stress and strain relaxation times. In this section, we determine the relaxed modulus M_{R} for a reference frequency f_{r}, a reference velocity v_{r} at this reference frequency and density ρ of the medium. By substituting $\omega_r = 2\pi f_r$ and $v_r = c_p(\omega_r)$ into the definition of phase velocity

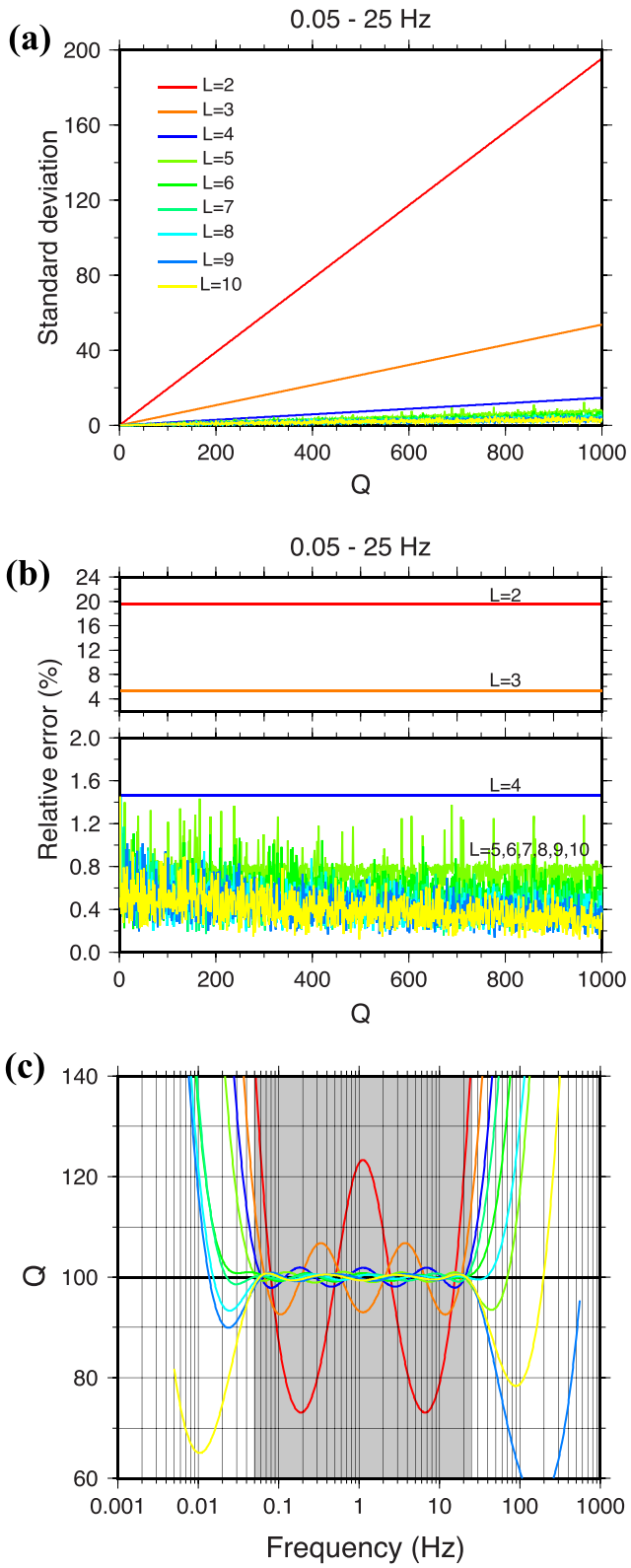

Figure 1. Parameter comparisons for inverted viscoelastic models with $L =$ 2–10 SLSs, including (a) standard deviation curves, (b) relative error curves and (c) Q-approximation curves for different L values. The frequency band of 0.05–25 Hz is labeled.

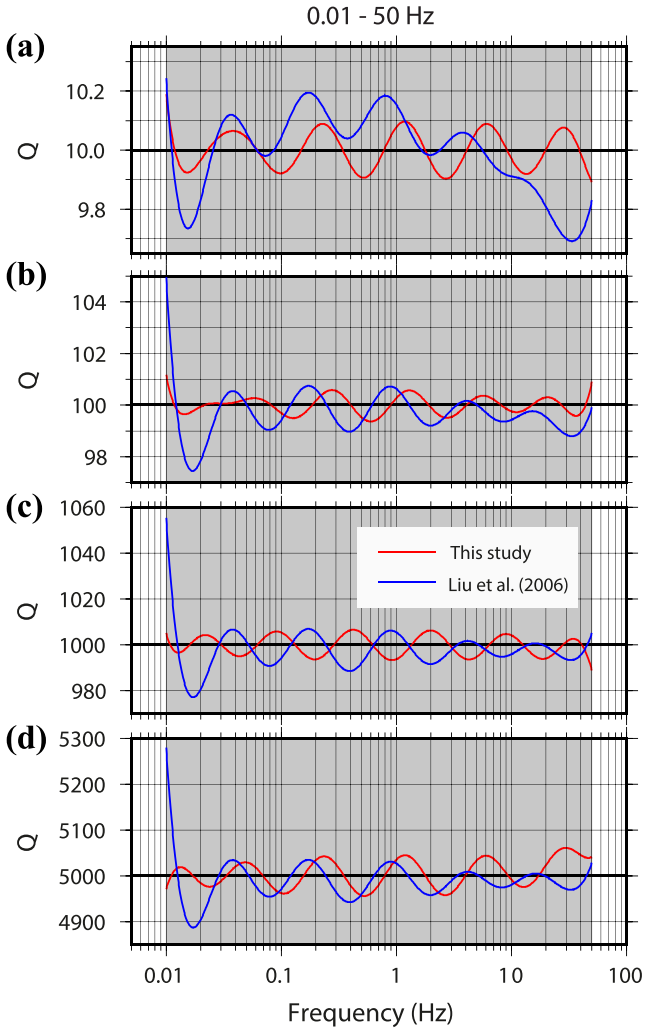

Figure 2. Comparison between Q models obtained using different approximations. The frequency band is 0.01–50 Hz. From (a) to (d), the Q values calculated for an eight-element viscoelastic model are 10, 100, 1000 and 5000, respectively. The red lines are for method proposed in this study and the blue lines are from Liu & Archuleta (2006).

c_p, that is, eq. (B2) (refer to Appendix B), we obtain the relaxed modulus

$$M_R = \rho \cdot v_r^2 \cdot \frac{\sqrt{\Theta_1{}^2 + \Theta_2{}^2} + \Theta_1}{2\left(\Theta_1{}^2 + \Theta_2{}^2\right)}, \tag{7-1}$$

where

$$\Theta_1 = 1 - L + \sum_{l=1}^{L} \frac{1 + \omega_r{}^2 \tau_{\varepsilon l} \tau_{\sigma l}}{1 + \omega_r{}^2 \tau_{\sigma l}{}^2}, \tag{7-2}$$

$$\Theta_2 = \sum_{l=1}^{L} \frac{\omega_r \left(\tau_{\varepsilon l} - \tau_{\sigma l}\right)}{1 + \omega_r{}^2 \tau_{\sigma l}{}^2}. \tag{7-3}$$

The relaxation function $G(t)$ describes the dynamic response of the medium. Using the equations in Appendix B, the relaxation function gives the phase and group velocities, which provide measurements of the attenuation–dispersion relationship in a viscoelastic model. To validate the viscoelastic model proposed in this study, the dispersion relationship generated by the GSLS is compared to the Kolsky–Futterman (K-F) dispersion relationship (Kolsky 1956; Futterman 1962; Ursin & Toverud 2002). For a set of parameters $Q = 100, f_r = 10$ Hz and $v_r = 3.0$ km s^{-1}, both the phase velocities and attenuation coefficients from these two models are compared in Fig. 3 as functions of frequency. The two sets of curves are highly consistent over the frequency band of interest, suggesting that our viscoelastic model meets the requirement for modeling seismic waves that propagates in viscoelastic models.

We also investigate how Q, f_r and v_r affect the phase and group velocities. For a reference velocity $v_r = 3.0$ km s^{-1} at different reference frequencies f_r, the phase and group velocities versus frequency for $Q = 60$, 80, 100, 120 and 140 and for $f_r = 0.1$, 1.0 and 10 Hz are illustrated in Fig. 4. The results demonstrate that low Q values tend to generate large velocity dispersions, which is consistent with a linear viscoelastic model. For the same Q value, different reference frequencies cause the dispersion curves to shift up and down.

3 VISCOELASTIC WAVE EQUATIONS

The 2-D first-order *P–SV* viscoelastic wave equations can be derived from the momentum conservation equation and viscoelastic constitutive relationship (for details, refer to Appendix A).

$$\rho \dot{v}_x = \frac{\partial \sigma_{xx}}{\partial x} + \frac{\partial \sigma_{xz}}{\partial x} + f_x, \tag{8-1}$$

$$\rho \dot{v}_z = \frac{\partial \sigma_{xz}}{\partial z} + \frac{\partial \sigma_{zz}}{\partial z} + f_z, \tag{8-2}$$

$$\dot{\sigma}_{xx} = \pi S_L^P \left(\frac{\partial v_x}{\partial x} + \frac{\partial v_z}{\partial z}\right) - 2\mu S_L^S \frac{\partial v_z}{\partial z} + T^P + T_{xx}^S, \tag{8-3}$$

$$\dot{\sigma}_{zz} = \pi S_L^P \left(\frac{\partial v_x}{\partial x} + \frac{\partial v_z}{\partial z}\right) - 2\mu S_L^S \frac{\partial v_x}{\partial x} + T^P + T_{zz}^S, \tag{8-4}$$

$$\dot{\sigma}_{xz} = \mu S_L^S \left(\frac{\partial v_z}{\partial x} + \frac{\partial v_x}{\partial z}\right) + T_{xz}^S, \tag{8-5}$$

$$\dot{r}_l^P = -\frac{1}{\tau_{\sigma l}^P}\left[r_l^P + \pi\left(\frac{\tau_{\varepsilon l}^P}{\tau_{\sigma l}^P} - 1\right)\left(\frac{\partial v_x}{\partial x} + \frac{\partial v_z}{\partial z}\right)\right], \tag{8-6}$$

$$\dot{r}_{xxl}^S = -\frac{1}{\tau_{\sigma l}^S}\left[r_{xxl}^S - 2\mu\left(\frac{\tau_{\varepsilon l}^S}{\tau_{\sigma l}^S} - 1\right)\frac{\partial v_z}{\partial z}\right], \tag{8-7}$$

$$\dot{r}_{zzl}^S = -\frac{1}{\tau_{\sigma l}^S}\left[r_{zzl}^S - 2\mu\left(\frac{\tau_{\varepsilon l}^S}{\tau_{\sigma l}^S} - 1\right)\frac{\partial v_x}{\partial x}\right], \tag{8-8}$$

$$\dot{r}_{xzl}^S = -\frac{1}{\tau_{\sigma l}^S}\left[r_{xzl}^S + \mu\left(\frac{\tau_{\varepsilon l}^S}{\tau_{\sigma l}^S} - 1\right)\left(\frac{\partial v_z}{\partial x} + \frac{\partial v_x}{\partial z}\right)\right], \tag{8-9}$$

where the definitions of the relevant variables and parameters are shown in Appendix A.

Similar to the numerical scheme used by Bayliss *et al.* (1986) and Xie & Yao (1988), we adopt the dimensional splitting method (Strang 1968) and MacCormack algorithm (Gottlieb & Turkel 1976) to construct the viscoelastic finite-difference scheme, which has an accuracy that is second order in time and fourth order in space. The MacCormack-type scheme dampens the spurious short-wavelength numerical (non-physical) noise generated by media discontinuities, computational-domain boundaries, grid discontinuities and other computational irregularities. Furthermore, the inherent dissipation can also eliminate the odd–even decoupling phenomenon

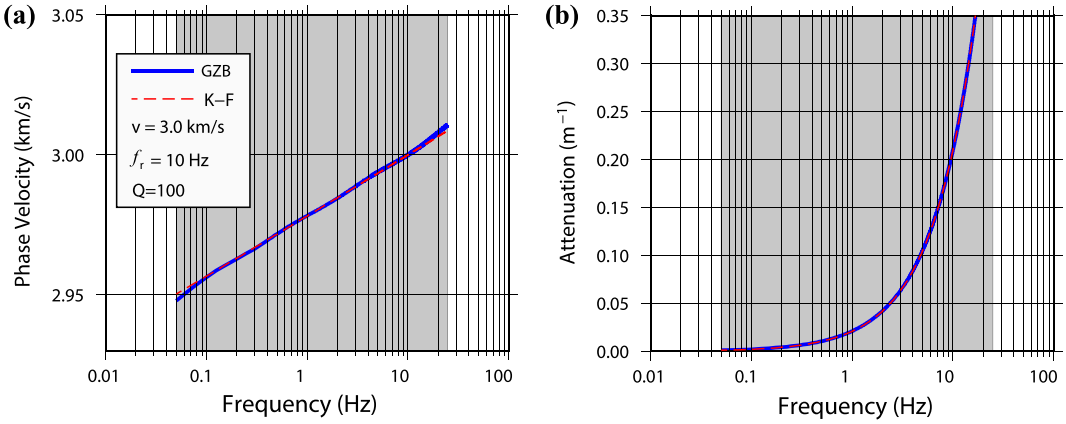

Figure 3. A dispersion comparison of the GZB model (blue line) and K-F model (red line), including (a) the phase velocity and (b) attenuation coefficient curves.

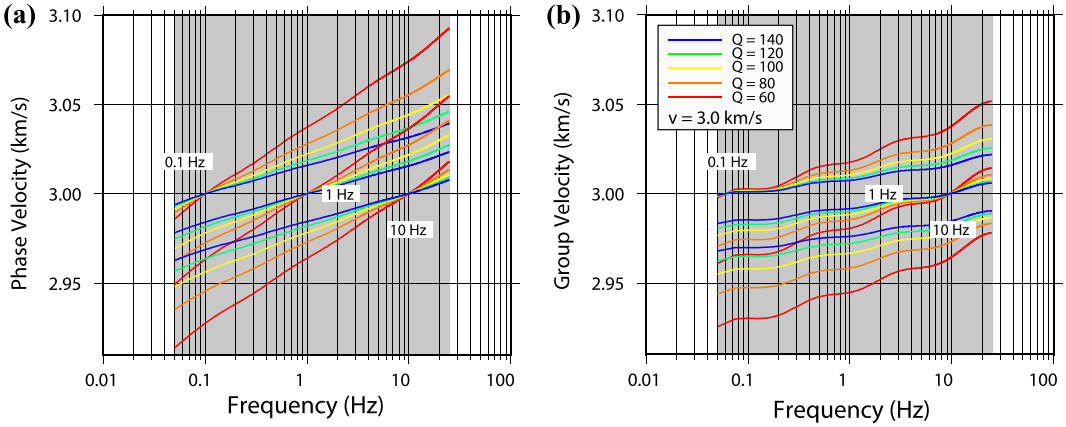

Figure 4. (a) Phase velocity and (b) group velocity curves calculated based on a model with a velocity of 3.0 km s^{-1} and $Q = 60$, 80, 100, 120 and 140 (colour lines) at $f_r = 0.1$, 1.0 and 10.0 Hz over the frequency range between 0.05 and 25 Hz.

(grid-to-grid oscillation) that exists in collocated-grid central finite-difference schemes (Zhang & Chen 2006; Zhang *et al.* 2012).

The vectorized form of eq. (8) can be written as

$$\frac{\partial U}{\partial t} = A\frac{\partial U}{\partial x} + B\frac{\partial U}{\partial z} + h, \tag{9}$$

where $U = (v_x\, v_z\, \sigma_{xx}\, \sigma_{zz}\, \sigma_{xz}\, r_1^P\, r_{xx1}^S\, r_{zz1}^S\, r_{xz1}^S \cdots r_4^P\, r_{xx4}^S\, r_{zz4}^S\, r_{xz4}^S)^T$ is the vector that composes of the velocities, stresses and memory variables. A and B are coefficient matrixes that consist of viscoelastic parameters. Additionally, $h = CU + S$, where C is the coefficient matrix related to the memory variables and S is the source term. A 2-D wave equation can be separated into two 1-D equations separately in the x- and z-directions using the dimensional splitting method. When assuming $f = AU$, the two 1-D partial differential equations have the similar form of

$$\frac{\partial U}{\partial t} = \frac{\partial f}{\partial x} + h. \tag{10}$$

For the standard first-order partial differential eq. (10), the MacCormack scheme has the iterative formulae (Gottlieb & Turkel 1976)

$$\bar{U}_i^n = U_i^n + \frac{\Delta t}{6\Delta x}\left[7\left(f_{i+1}^n - f_i^n\right) - \left(f_{i+2}^n - f_{i+1}^n\right)\right] + \Delta t \cdot h_i^n, \tag{11-1}$$

Table 1. Model parameters used in this study.

Layer	Depth (km)	Density (g cm^{-3})	V_P (km s^{-1})	V_S (km s^{-1})	Q_P	Q_S
1st	15.00	1.80	3.00	1.50	80	40
2nd	∞	2.20	6.00	3.14	120	60

$$U_i^{n+1} = \frac{1}{2}\left\{U_i^n + \bar{U}_i + \frac{\Delta t}{6\Delta x}\left[7\left(\bar{f}_i - \bar{f}_{i-1}\right) - \left(\bar{f}_{i-1} - \bar{f}_{i-2}\right)\right]\right\} + \frac{\Delta t}{2}\bar{h}_i^n, \tag{11-2}$$

with the stable condition $\frac{\Delta t}{\Delta x}c_{\max} \le \frac{2}{3}$, where $c_{\max}$ is the highest phase velocity of the medium, namely, the unrelaxation velocity at infinite frequency $c_{\max} = c_u = \sqrt{\frac{M_R}{\rho}\left(1 - L + \sum_{l=1}^{L}\frac{\tau_{\varepsilon l}}{\tau_{\sigma l}}\right)}$.

The free-surface boundary condition severely affects the accuracy of waveforms at the free surface, particularly for surface waves (Kosloff & Carcione 2010). We extend the Stress Image Method to the viscoelastic equations. The Stress Image Method keeps the stresses and memory variables antisymmetric about a planar surface in the vertical direction, while updating the velocity components of ghost gridpoints above the free surface (Levander 1988; Robertsson 1996). Assuming that the free-surface boundary is set at $j = 0$ and z-axis is downward positive, the stress and memory variables satisfy

$$\sigma_{zz}|_{j=0} = \sigma_{xz}|_{j=0} = 0, \tag{12-1}$$

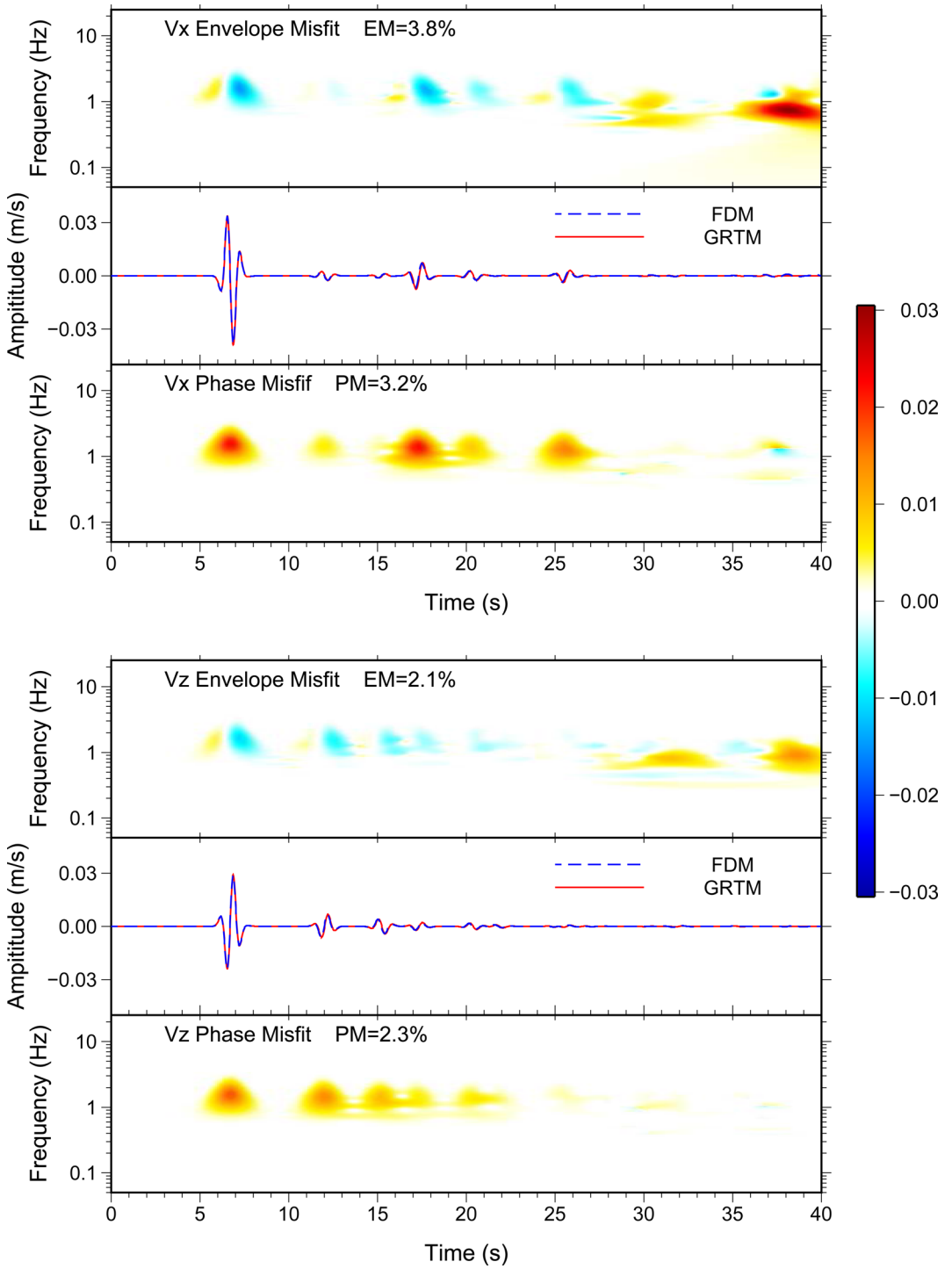

Figure 5. Waveform comparisons between FDM (dashed blue line) and GRTM (solid red line) for horizontal (upper three panels) and vertical (lower three panels) component records at a receiver located at 10 km from the source. The time–frequency envelope misfit (EM) and phase misfit (PM) were calculated using the TF_MISFIT_GOF_CRITERIA package (Kristeková *et al*. 2009).

$$r_l^P\big|_{j=0} = r_{zzl}^S\big|_{j=0} = r_{xzl}^S\big|_{j=0} = 0, \tag{12-2}$$

where $r_l^P|_{j=0} = 0$ is only valid for the wave equation of σ_{zz} in eq. (8-4).

In the ghost-grid layers $j < 0$, the stresses satisfy

$$\sigma_{zz}|_{j=-1} = -\sigma_{zz}|_{j=1}, \quad \sigma_{xz}|_{j=-1} = -\sigma_{xz}|_{j=1}, \tag{13-1}$$

$$\sigma_{zz}|_{j=-2} = -\sigma_{zz}|_{j=2}, \quad \sigma_{xz}|_{j=-2} = -\sigma_{xz}|_{j=2}. \tag{13-2}$$

Because σ_{xz} and σ_{zz} equal to zero at $j = 0$, the velocities satisfy

$$\frac{\partial v_x}{\partial z} + \frac{\partial v_z}{\partial x} = 0, \tag{14-1}$$

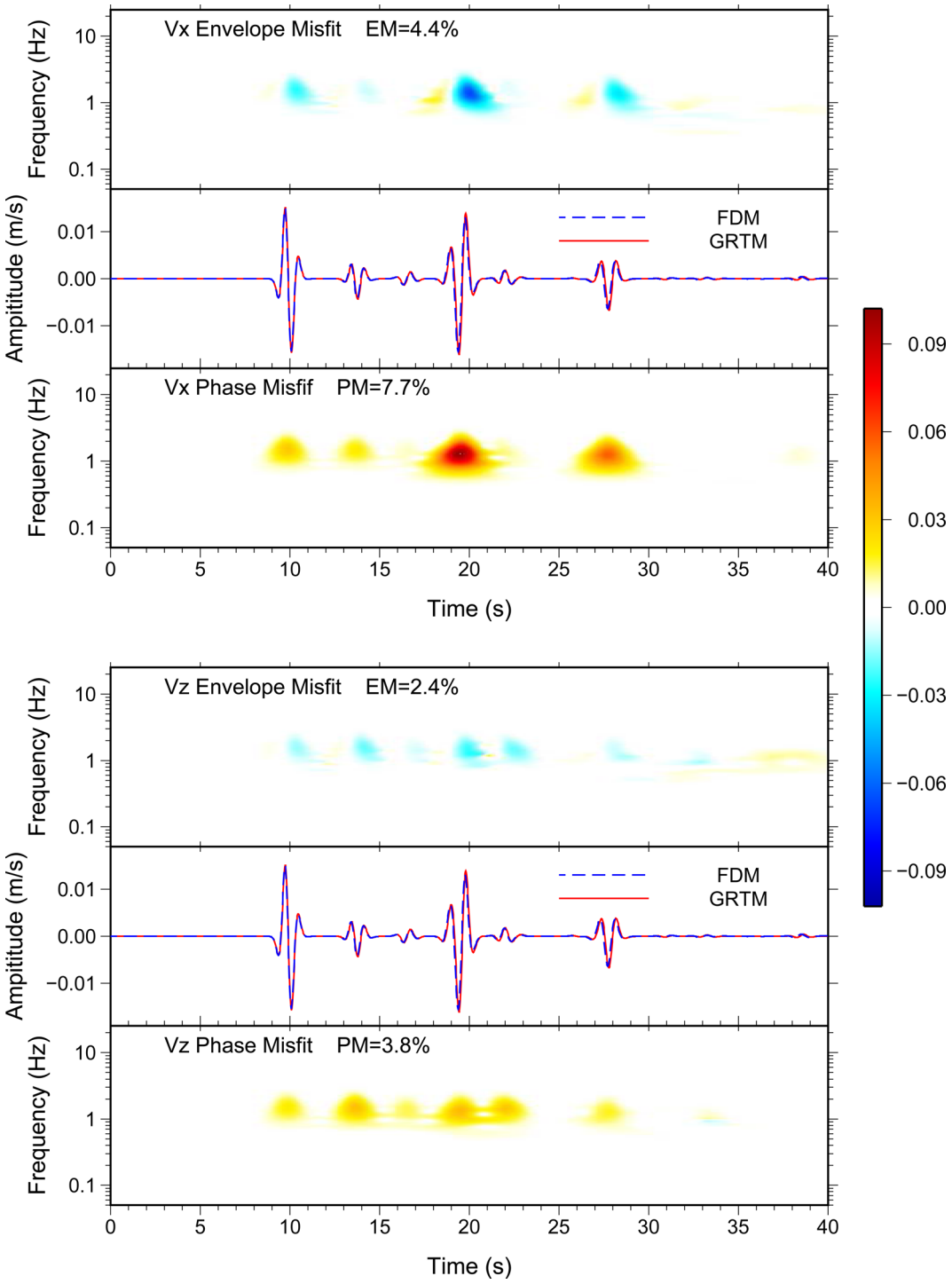

Figure 6. Similar to Fig. 5, waveform comparisons between FDM and GRTM for records at a receiver located 20 km from the source.

$$\pi S_L^P \left(\frac{\partial v_x}{\partial x} + \frac{\partial v_z}{\partial z} \right) - 2\mu S_L^S \frac{\partial v_x}{\partial x} = 0, \tag{14-2}$$

where all relevant parameters are shown in eq. (8). Fourth-order central difference is used for horizontal derivatives $\frac{\partial v_x}{\partial x}$ and $\frac{\partial v_z}{\partial x}$. Second-order and fourth-order schemes are used for vertical derivatives $\frac{\partial v_x}{\partial z}$ and $\frac{\partial v_z}{\partial z}$ to obtain v_x and v_z at ghost-grid layers $j = -1$ and -2. At three remaining artificial boundaries, the damping boundary of Cerjan *et al*. (1985) are adopted.

4 NUMERICAL VALIDATION

To validate the viscoelastic modeling method proposed in this study, we compare our result with an analytical benchmark solution. Based on the correspondence principle (Bland 1960), the dynamic solution for a viscoelastic model can be obtained from the solution of the corresponding elastic model by Fourier transform of the elastic solution to the frequency domain, replacement of the elastic constants with the corresponding viscoelastic complex moduli and transformation back to the time domain. We use the GRTM (Yao

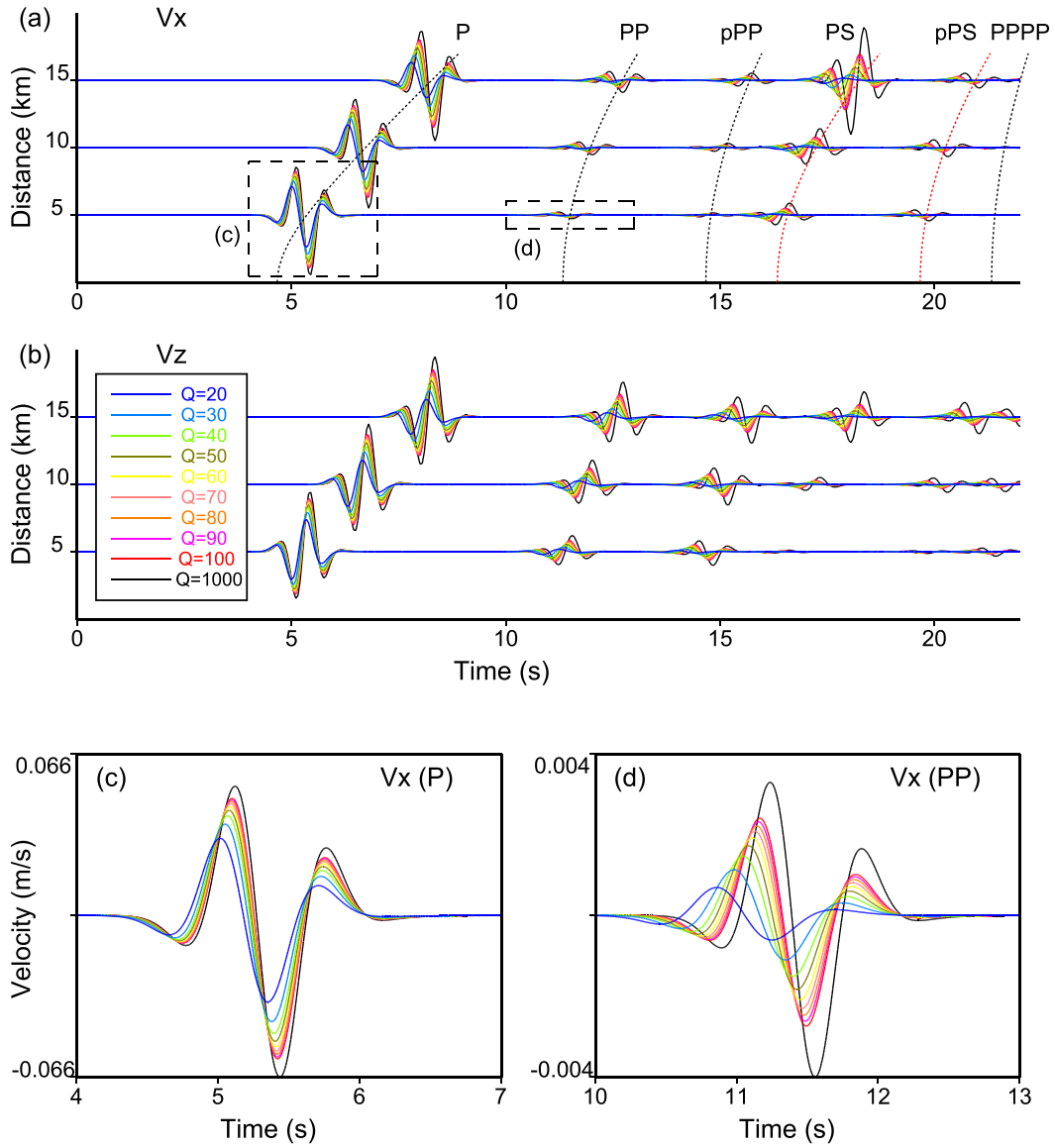

Figure 7. Simulated waveforms using FDM at reference frequency $f_r = 0.1$ Hz. The colours indicate different Q values between 20 and 1000. The (a) horizontal and (b) vertical component velocities are recorded at epicentral distances of 5, 10 and 15 km. The dashed rectangles in (a) indicate the regional waveforms, which we amplified to explicitly display the details for the (c) direct P waves and (d) reflected P waves.

& Harkrider 1983; Chen 1993, 1999) to compute synthetic seismograms in 2-D multilayered elastic media and convert them into viscoelastic solutions.

The 2-D simulation is implemented in a two-layer model with a size of 60 × 60 km and its parameters listed in Table 1. The source is located at a depth of 5 km, and synthetic seismograms are calculated at two surface locations with epicentral distances of 10 and 20 km. The source mechanism is a 2-D explosion with a scalar moment $m_0 = 1 \times 10^{15}$ N m. The source time function is a Ricker wavelet with a centre frequency $f_c = 1.0$ Hz and a time-shift of 3.0 s. The fine time and space intervals $dt = 0.005$ s and $dx = dz = 0.05$ km are used to suppress the numerical dispersion. The grid size of the discretized model is 1200 × 1200. The maximum frequency of the Ricker wavelet is estimated to be 2.5 times the centre frequency and the minimum sampling rate per wavelength (PPW $\sim \frac{0.92 v_s}{2.5 \cdot f_c \cdot dx}$) can reach 11. We set $f_r = 10$ Hz, and the Q values are $Q_P = 80$ and $Q_S = 40$ for the first layer and $Q_P = 100$ and $Q_S = 60$ for the second layer.

To quantitatively assess the consistency of synthetic seismograms from two different methods, we use the misfit criteria developed by Kristeková *et al*. (2006) to investigate the time–frequency misfit and goodness of fit between the two sets of seismograms. The misfit criteria include the time–frequency envelope (EM) and phase misfits (PM), time-dependent EM and PM, frequency-dependent EM and PM and single-valued EM and PM. The advantage of the joint time–frequency judgment is that it can separate the EM and PM, while providing the misfit information simultaneously in both the time and frequency domains. The misfit criteria for the 'excellent' level suggested in Kristeková *et al*. (2009) are ±0.22 for the EM, ±0.2 for the PM and 8 for the goodness-of-fit value. All comparisons between FDM and GRTM solutions in this study fall within the 'excellent' level. Here, we present the time–frequency EM and PM comparisons and the global measurements of the agreement between the two solutions, including the single-valued EM, PM, envelope goodness of fit (EG) and phase goodness of fit (PG), all of which are calculated using the TF_MISFIT_GOF_CRITERIA package (Kristeková *et al*.

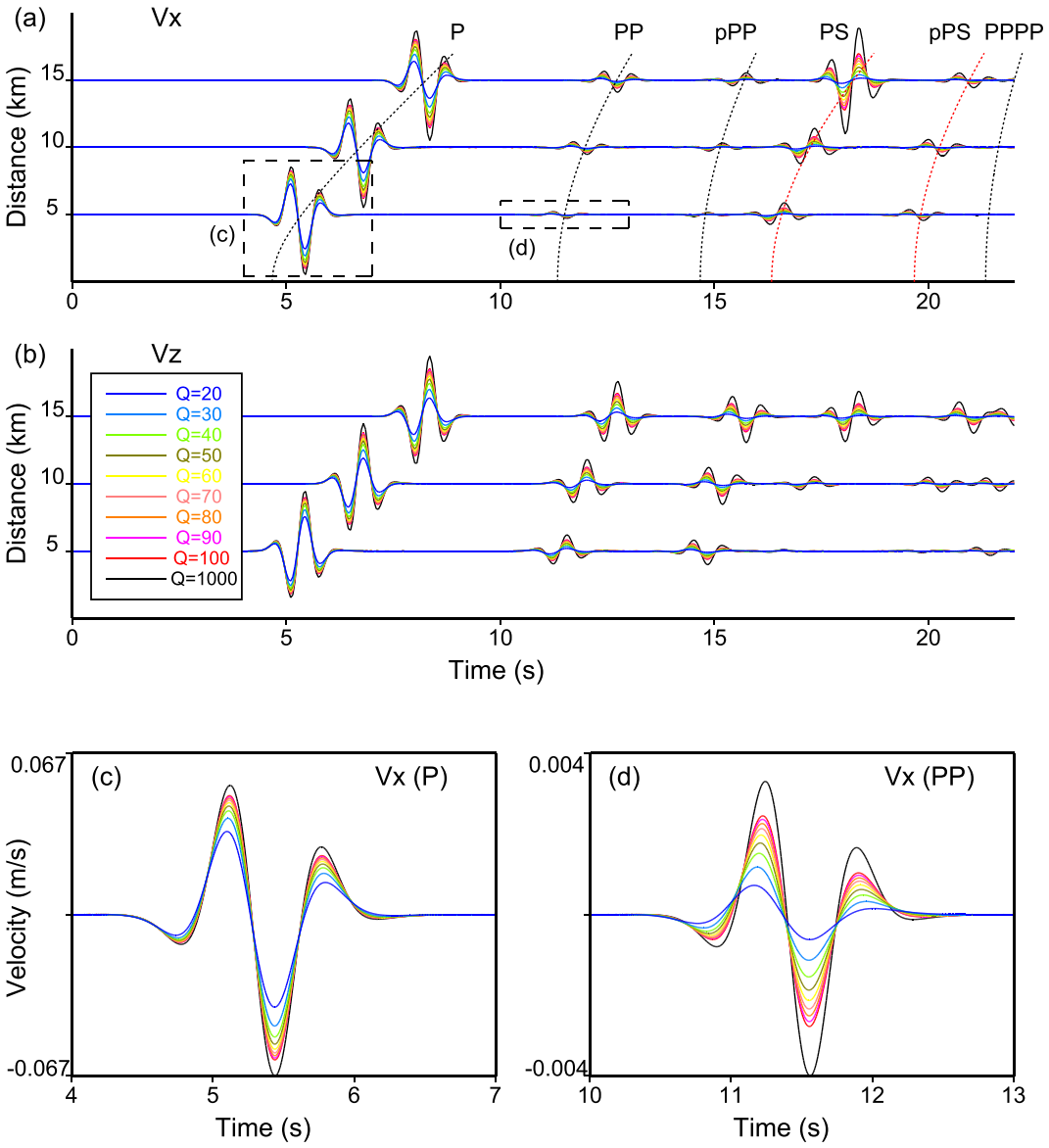

Figure 8. Similar to Fig. 7, but for reference frequency $f_r = 1.0$ Hz.

2009). Figs 5 and 6 show the time–frequency misfit and goodness-of-fit at epicentral distances of 10 and 20 km, respectively. The errors over the specified frequency range are less than 10 per cent, and EG and PG, which represent the degree of agreement, are both greater than 8. These values indicate that the two sets of results have excellent levels of accordance.

Based on the two-layer model used in Section 2.2 to investigate the effects of both Q and f_r on dispersion, we compare synthetic seismograms for different Q and f_r. Figs 7–9 show the waveforms for $Q_P = Q_S = 20$, 30, 40, 50, 60, 70, 80, 90, 100 and 1000 and $f_r = 0.1$, 1.0 and 10 Hz. The waveforms for $Q = 1000$ can be considered to be a near-elastic model. The strong attenuation that results from small Q values severely changes the amplitude and frequency content of seismograms. As Q decreases, the amplitude decreases and the signal becomes wider, due to the loss of high-frequency contents. As mentioned above, the causal relationship requires the attenuation be accompanied by dispersion. However, the absolute phase velocity still depends on the selected reference frequency, at which the phase velocity does not change. If f_r is chosen to be smaller than the dominant frequency band of the signal, the attenuation causes the signal to arrive earlier. By contrast, if f_r is larger than the dominant frequency band, the attenuation can delay the arrivals of the signal. The actual f_r should be higher than the main frequency band of the signal of interest.

5 DISCUSSION AND CONCLUSIONS

We constructed a viscoelastic model and proposed a four-SLS viscoelastic model with a trade-off between accuracy and efficiency. Additionally, we adopted a new strategy in which the Q approximation procedure was separated from the simulation procedure. We built a database that limited the Q to discrete values over a range of 2–1000, which tremendously reduced the number of related viscoelastic parameters in the calculation. Thus, the finite-difference calculation could directly obtain the corresponding viscoelastic parameters by calling the database, which greatly reduced the computation time for modeling.

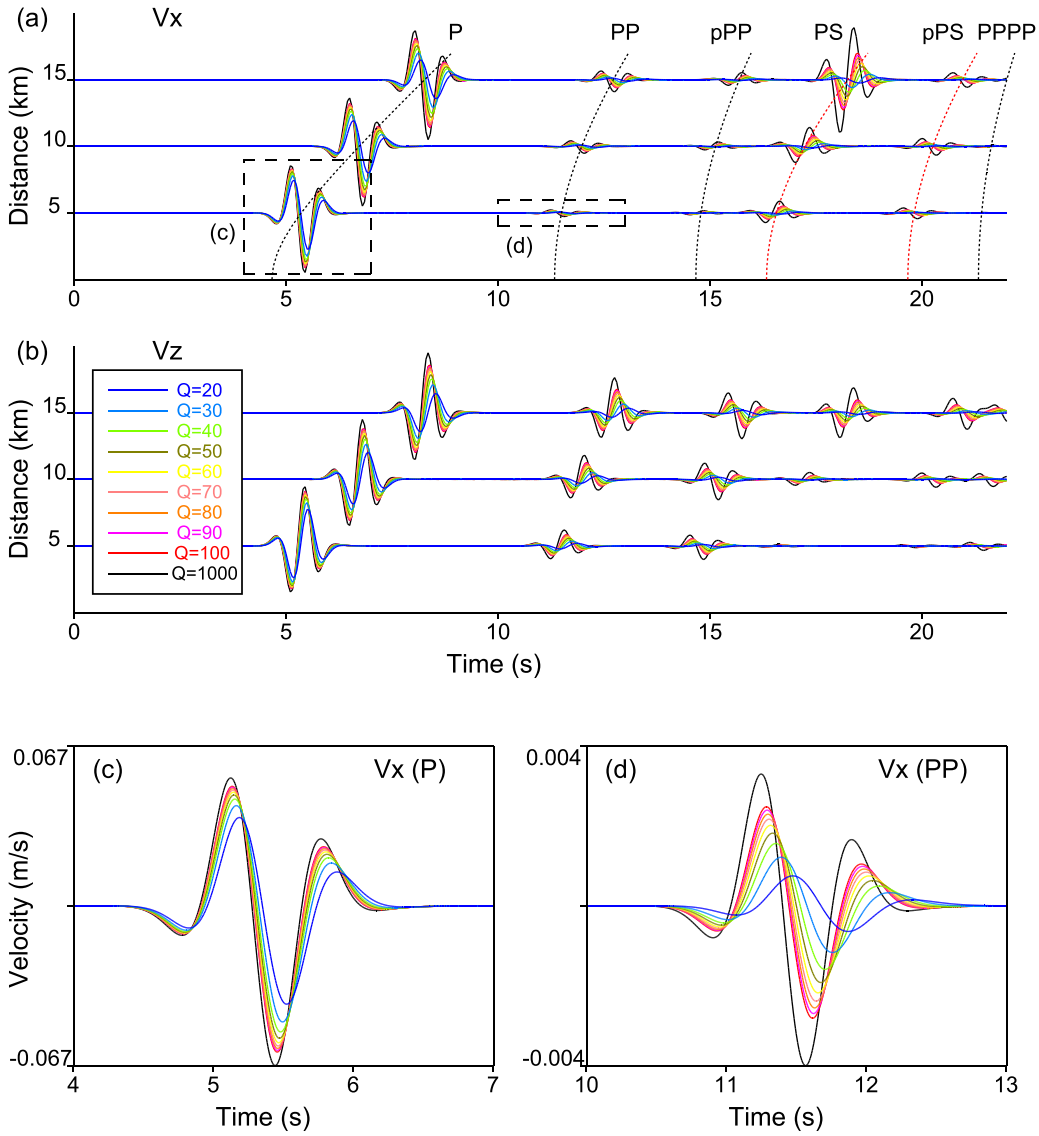

Figure 9. Similar to Fig. 7, but for reference frequency $f_r = 10.0$ Hz.

We reformulated expressions of memory variables by separating the *P*- and *S*-wave variables. We implemented 2-D time-domain finite-difference viscoelastic modeling and validated the results by comparing them with analytical solutions calculated using the GRTM. The effects of both Q and f_r on waveforms were verified. Low Q values tended to attenuate more high-frequency content than low-frequency content, thus reducing the signal amplitude and lowering the dominant frequency. Additionally, choosing the reference frequency affected the arrival times of the signals. To simulate the actual dispersion relationship in the real Earth, we suggest that the reference frequency should be larger than the dominant frequency band of the signal.

ACKNOWLEDGEMENTS

We are grateful to Prof X. Chen and Dr H. Zhang for providing the 2-D elastic GRTM code to calculate the synthetic seismograms and for fruitful discussions. Two anonymous reviewers are appreciated for their constructive comments that greatly improved this manuscript. The parallel calculations of the viscoelastic modeling were completed on clusters at the Computer Simulation Lab, IGGCAS. This research was supported by the National Natural Science Foundation of China (grants 41174048, 41374065 and 41374045).

REFERENCES

Aki, K. & Richards, P.G., 1980. *Quantitative Seismology: Theory and Method,* W.H. Freeman, 932 pp.

Bayliss, A., Jordan, K., LeMesurier, B. & Turkel, E., 1986. A fourth-order accurate finite-difference scheme for the computation of elastic waves, *Bull. seism. Soc. Am.,* **76,** 1115–1132.

Blanch, J.O., Robertsson, J.O. & Symes, W.W., 1995. Modeling of a constant Q: methodology and algorithm for an efficient and optimally inexpensive viscoelastic technique, *Geophysics,* **60,** 176–184.

Bland, D.R., 1960. *The Theory of Linear Viscoelasticity,* Pergamon Press.

Bohlen, T., 2002. Parallel 3-D viscoelastic finite difference seismic modelling, *Comp. Geosci.,* **28,** 887–899.

Cao, D. & Yin, X., 2014. Equivalence relations of generalized rheological models for viscoelastic seismic-wave modeling, *Bull. seism. Soc. Am.,* **104,** 260–268.

Carcione, J.M., 1993. Seismic modeling in viscoelastic media, *Geophysics,* **58,** 110–120.

Carcione, J.M., 2008. Theory and modeling of constant-Q *P*- and *S*-waves using fractional time derivatives, *Geophysics,* **74,** T1–T11.
Carcione, J.M., 2010. A generalization of the Fourier pseudospectral method, *Geophysics,* **75,** A53–A56.
Carcione, J.M., Cavallini, F., Mainardi, F. & Hanyga, A., 2002. Time-domain modeling of constant-Q seismic waves using fractional derivatives, *Pure appl. Geophys.,* **159,** 1719–1736.
Carcione, J.M., Kosloff, D. & Kosloff, R., 1988a. Viscoacoustic wave propagation simulation in the earth, *Geophysics,* **53,** 769–777.
Carcione, J.M., Kosloff, D. & Kosloff, R., 1988b. Wave propagation simulation in a linear viscoacoustic medium, *Geophys. J. Int.,* **93,** 393–401.
Carcione, J.M., Kosloff, D. & Kosloff, R., 1988c. Wave propagation simulation in a linear viscoelastic medium, *Geophys. J. Int.,* **95,** 597–611.
Cerjan, C., Kosloff, D., Kosloff, R. & Reshef, M., 1985. A nonreflecting boundary condition for discrete acoustic and elastic wave equations, *Geophysics,* **50**(4), 705–708.
Chen, X., 1993. A systematic and efficient method of computing normal modes for multilayered half-space, *Geophys. J. Int.,* **115,** 391–409.
Chen, X., 1999. Seismogram synthesis in multi-layered half-space. Part I. Theoretical formulations, *Earthq. Res. China,* **13,** 149–174.
Chen, W. & Holm, S., 2004. Fractional Laplacian time-space models for linear and nonlinear lossy media exhibiting arbitrary frequency power-law dependency, *J. acoust. Soc. Am.,* **115,** 1424–1430.
Christensen, R.M., 1982. *Theory of Viscoelasticity,* Academic Press.
Day, S.M. & Bradley, C.R., 2001. Memory-efficient simulation of anelastic wave propagation, *Bull. seism. Soc. Am.,* **91,** 520–531.
Day, S.M. & Minster, J.B., 1984. Numerical simulation of attenuated wavefields using a Padé approximant method, *Geophys. J. Int.,* **78,** 105–118.
Emmerich, H. & Korn, M., 1987. Incorporation of attenuation into time-domain computations of seismic wave fields, *Geophysics,* **52,** 1252–1264.
Futterman, W.I., 1962. Dispersive body waves, *J. geophys. Res.,* **67,** 5279–5291.
Gottlieb, D. & Turkel, E., 1976. Dissipative two-four methods for time-dependent problems, *Math. Comput.,* **30,** 703–723.
Hestholm, S.O., 1999. Three-dimensional finite difference viscoelastic wave modelling including surface topography, *Geophys. J. Int.,* **139,** 852–878.
Hestholm, S.O. & Ruud, B.O., 2000. 2-D finite-difference viscoelastic wave modelling including surface topography, *Geophys. Prospect.,* **48,** 341–373.
Ingber, L., 1989. Very fast simulated re-annealing, *Math. Comput. Model.,* **12,** 967–973.
Kjartansson, E., 1979. Constant Q-wave propagation and attenuation, *J. geophys. Res.,* **84,** 4737–4748.
Kolsky, H., 1956. The propagation of stress pulses in viscoelastic solids, *Phil. Mag.,* **1,** 693–710.
Komatitsch, D. & Tromp, J., 1999. Introduction to the spectral element method for three-dimensional seismic wave propagation, *Geophys. J. Int.,* **139,** 806–822.
Kosloff, D. & Carcione, J.M., 2010. Two-dimensional simulation of Rayleigh waves with staggered sine/cosine transforms and variable grid spacing, *Geophysics,* **75,** T133–T140.
Krebes, E. & Quiroga-Goode, G., 1994. A standard finite-difference scheme for the time-domain computation of anelastic wavefields, *Geophysics,* **59,** 290–296.
Kristek, J. & Moczo, P., 2003. Seismic-wave propagation in viscoelastic media with material discontinuities: a 3D fourth-order staggered-grid finite-difference modeling, *Bull. seism. Soc. Am.,* **93,** 2273–2280.
Kristeková, M., Kristek, J. & Moczo, P., 2009. Time-frequency misfit and goodness-of-fit criteria for quantitative comparison of time signals, *Geophys. J. Int.,* **178,** 813–825.
Kristeková, M., Kristek, J., Moczo, P. & Day, S.M., 2006. Misfit criteria for quantitative comparison of seismograms, *Bull. seism. Soc. Am.,* **96,** 1836–1850.
Levander, A.R., 1988. Fourth-order finite-difference P-SV seismograms, *Geophysics,* **53,** 1425–1436.
Liu, P. & Archuleta, R.J., 2006. Efficient modeling of Q for 3D numerical simulation of wave propagation, *Bull. seism. Soc. Am.,* **96,** 1352–1358.
Liu, H.P., Anderson, D.L. & Kanamori, H., 1976. Velocity dispersion due to anelasticity; implications for seismology and mantle composition, *Geophys. J. R. astr. Soc.,* **47,** 41–58.
Moczo, P. & Kristek, J., 2005. On the rheological models used for time-domain methods of seismic wave propagation, *Geophys. Res. Lett.,* **32,** L01306, doi:10.1029/2004GL021598.
Murphy, W.F., III, 1982. Effects of partial water saturation on attenuation in Massilon sandstone and Vycor porous glass, *J. acoust. Soc. Am.,* **71,** 1458–1468.
O'connell, R. & Budiansky, B., 1978. Measures of dissipation in viscoelastic media, *Geophys. Res. Lett.,* **5,** 5–8.
Robertsson, J.O., 1996. A numerical free-surface condition for elastic/viscoelastic finite-difference modeling in the presence of topography, *Geophysics,* **61,** 1921–1934.
Robertsson, J.O., Blanch, J.O. & Symes, W.W., 1994. Viscoelastic finite-difference modeling, *Geophysics,* **59,** 1444–1456.
Saenger, E.H. & Bohlen, T., 2004. Finite-difference modeling of viscoelastic and anisotropic wave propagation using the rotated staggered grid, *Geophysics,* **69,** 583–591.
Samec, P. & Blangy, J., 1992. Viscoelastic attenuation, anisotropy, and AVO, *Geophysics,* **57,** 441–450.
Spencer, J.W., Jr, 1981. Stress relaxations at low frequencies in fluid-saturated rocks: attenuation and modulus dispersion, *J. geophys. Res.,* **86,** 1803–1812.
Strang, G., 1968. On the construction and comparison of difference schemes, *SIAM J. Numer. Anal.,* **5,** 506–517.
Szu, H. & Hartley, R., 1987. Fast simulated annealing, *Phys. Lett. A,* **122,** 157–162.
Tal-Ezer, H., Carcione, J. & Kosloff, D., 1990. An accurate and efficient scheme for wave propagation in linear viscoelastic media, *Geophysics,* **55,** 1366–1379.
Treeby, B.E. & Cox, B., 2010. Modeling power law absorption and dispersion for acoustic propagation using the fractional Laplacian, *J. acoust. Soc. Am.,* **127,** 2741–2748.
Ursin, B. & Toverud, T., 2002. Comparison of seismic dispersion and attenuation models, *Stud. Geophys. Geod.,* **46,** 293–320.
Wang, Y., 2009. *Seismic Inverse Q Filtering,* Wiley-Blackwell.
Xie, X. & Yao, Z., 1988. *P-SV* wave responses for a point source in two-dimensional heterogeneous media: finite-difference method, *Chin. J. Geophys.,* **31,** 473–493.
Xu, T. & McMechan, G.A., 1995. Composite memory variables for viscoelastic synthetic seismograms, *Geophys. J. Int.,* **121,** 634–639.
Yao, Z. & Harkrider, D., 1983. A generalized reflection-transmission coefficient matrix and discrete wavenumber method for synthetic seismograms, *Bull. seism. Soc. Am.,* **73,** 1685–1699.
Zhang, W. & Chen, X., 2006. Traction image method for irregular free surface boundaries in finite difference seismic wave simulation, *Geophys. J. Int.,* **167,** 337–353.
Zhang, W., Shen, Y. & Zhao, L., 2012. Three-dimensional anisotropic seismic wave modelling in spherical coordinates by a collocated-grid finite-difference method, *Geophys. J. Int.,* **188,** 1359–1381.
Zhu, T. & Carcione, J.M., 2014. Theory and modelling of constant-Q *P*- and *S*-waves using fractional spatial derivatives, *Geophys. J. Int.,* **196,** 1787–1795.
Zhu, T. & Harris, J.M., 2014. Modeling acoustic wave propagation in heterogeneous attenuating media using decoupled fractional Laplacians, *Geophysics,* **79,** T105–T116.

APPENDIX A: DERIVATION OF THE FIRST-ORDER VISCOELASTIC WAVE EQUATION

The constitutive relationship eq. (1) for a linear elastic or viscoelastic material can be described as

$$\sigma_{ij} = G_{ijkl} * \dot{\varepsilon}_{kl} = \dot{G}_{ijkl} * \varepsilon_{kl} \tag{A1}$$

where $*$ denotes the convolution by which each strain history $\dot{\varepsilon}_{ij}$ can be transformed into the current stress value $\sigma_{ij}(t)$. The dot denotes

a time derivative and G is a fourth-order tensor called the relaxation function. For an isotropic material, G degenerates into a second-order tensor function and the constitutive relationship simplifies to (Christensen 1982)

$$\sigma_{ij} = \dot{\Lambda} * \delta_{ij}\varepsilon_{kk} + 2\dot{\mathrm{M}} * \varepsilon_{ij}, \tag{A2}$$

where δ_{ij} is the Kronecker delta and Einstein's summation convention is used. Λ and M are the bulk and shear relaxation functions, respectively. We define

$$\prod = \Lambda + 2\mathrm{M} \tag{A3}$$

and use the standard linear solid model for Π and M, that is,

$$\prod = \pi\left(1 - \sum_{l=1}^{L}\left(1 - \frac{\tau_{\varepsilon l}^{P}}{\tau_{\sigma l}^{P}}\right)e^{-t/\tau_{\sigma l}^{P}}\right)\theta\left(t\right), \tag{A4}$$

$$\mathrm{M} = \mu\left(1 - \sum_{l=1}^{L}\left(1 - \frac{\tau_{\varepsilon l}^{S}}{\tau_{\sigma l}^{S}}\right)e^{-t/\tau_{\sigma l}^{S}}\right)\theta\left(t\right), \tag{A5}$$

where $\pi = \lambda + 2\mu$ and λ and μ are the elastic Lamé parameters, which describe the relaxation modulus of the medium. $\tau_{\sigma l}^{P}$ and $\tau_{\varepsilon l}^{P}$ are the stress and strain relaxation times for P waves, while $\tau_{\sigma l}^{S}$ and $\tau_{\varepsilon l}^{S}$ are the stress and strain relaxation times for S waves. $\theta\left(t\right)$ is the Heaviside function and L is the number of standard linear solids connected in parallel to model the relaxation functions. In this study, we choose the optimal number $L = 4$.

Using the time derivative of the definition of strain,

$$\dot{\varepsilon}_{ij} = \frac{1}{2}\left(\partial_i v_j + \partial_j v_i\right), \tag{A6}$$

where $\partial_i v_j$ is the partial derivative applied on the jth velocity component along the ith direction.

From the constitutive relationship,

$$\dot{\sigma}_{ij} = \delta_{ij}\left(\dot{\prod} - 2\dot{\mathrm{M}}\right) * \partial_k v_k + \dot{\mathrm{M}} * \left(\partial_i v_j + \partial_j v_i\right). \tag{A7}$$

By inserting the standard linear solid expressions (add number of equations) for Π and M and performing the time differentiation for each of their factors, substituting i, j for x, z, we obtain

$$\begin{aligned}\dot{\sigma}_{xx} = &\left\{\pi\left[1 - \sum_{l=1}^{L}\left(1 - \frac{\tau_{\varepsilon l}^{P}}{\tau_{\sigma l}^{P}}\right)\right] - 2\mu\left[1 - \sum_{l=1}^{L}\left(1 - \frac{\tau_{\varepsilon l}^{S}}{\tau_{\sigma l}^{S}}\right)\right]\right\}\\ &\times\left(\frac{\partial v_x}{\partial x} + \frac{\partial v_z}{\partial z}\right) + 2\mu\left[1 - \sum_{l=1}^{L}\left(1 - \frac{\tau_{\varepsilon l}^{S}}{\tau_{\sigma l}^{S}}\right)\right]\frac{\partial v_x}{\partial x}\\ &+ \sum_{l=1}^{L} r_{xxl}^{P} + \sum_{l=1}^{L} r_{xxl}^{S}\end{aligned} \tag{A8}$$

$$\begin{aligned}\dot{\sigma}_{zz} = &\left\{\pi\left[1 - \sum_{l=1}^{L}\left(1 - \frac{\tau_{\varepsilon l}^{P}}{\tau_{\sigma l}^{P}}\right)\right] - 2\mu\left[1 - \sum_{l=1}^{L}\left(1 - \frac{\tau_{\varepsilon l}^{S}}{\tau_{\sigma l}^{S}}\right)\right]\right\}\\ &\times\left(\frac{\partial v_x}{\partial x} + \frac{\partial v_z}{\partial z}\right) + 2\mu\left[1 - \sum_{l=1}^{L}\left(1 - \frac{\tau_{\varepsilon l}^{S}}{\tau_{\sigma l}^{S}}\right)\right]\frac{\partial v_z}{\partial z}\\ &+ \sum_{l=1}^{L} r_{zzl}^{P} + \sum_{l=1}^{L} r_{zzl}^{S}\end{aligned} \tag{A9}$$

$$\dot{\sigma}_{xz} = \mu\left[1 - \sum_{l=1}^{L}\left(1 - \frac{\tau_{\varepsilon l}^{S}}{\tau_{\sigma l}^{S}}\right)\right]\left(\frac{\partial v_z}{\partial x} + \frac{\partial v_x}{\partial z}\right) + \sum_{l=1}^{L} r_{xzl}^{S}, \tag{A10}$$

where

$$r_{xxl}^{P} = \pi\frac{1}{\tau_{\sigma l}^{P}}\left(1 - \frac{\tau_{\varepsilon l}^{P}}{\tau_{\sigma l}^{P}}\right)e^{-t/\tau_{\sigma l}^{P}}\theta\left(t\right) * \left(\frac{\partial v_x}{\partial x} + \frac{\partial v_z}{\partial z}\right), \tag{A11}$$

$$r_{xxl}^{S} = -2\mu\frac{1}{\tau_{\sigma l}^{S}}\left(1 - \frac{\tau_{\varepsilon l}^{S}}{\tau_{\sigma l}^{S}}\right)e^{-t/\tau_{\sigma l}^{S}}\theta\left(t\right) * \frac{\partial v_z}{\partial z}, \tag{A12}$$

$$r_{zzl}^{P} = \pi\frac{1}{\tau_{\sigma l}^{P}}\left(1 - \frac{\tau_{\varepsilon l}^{P}}{\tau_{\sigma l}^{P}}\right)e^{-t/\tau_{\sigma l}^{P}}\theta\left(t\right) * \left(\frac{\partial v_x}{\partial x} + \frac{\partial v_z}{\partial z}\right), \tag{A13}$$

$$r_{zzl}^{S} = -2\mu\frac{1}{\tau_{\sigma l}^{S}}\left(1 - \frac{\tau_{\varepsilon l}^{S}}{\tau_{\sigma l}^{S}}\right)e^{-t/\tau_{\sigma l}^{S}}\theta\left(t\right) * \frac{\partial v_x}{\partial x}, \tag{A14}$$

$$r_{xzl}^{S} = \mu\frac{1}{\tau_{\sigma l}^{S}}\left(1 - \frac{\tau_{\varepsilon l}^{S}}{\tau_{\sigma l}^{S}}\right)e^{-t/\tau_{\sigma l}^{S}}\theta\left(t\right) * \left(\frac{\partial v_z}{\partial x} + \frac{\partial v_x}{\partial z}\right), \tag{A15}$$

are the memory variables, with the subscript $l \in [1, L]$.

The expressions of r_{xxl}^{P} and r_{zzl}^{P} are identical and can be converted into a single expression:

$$r_{l}^{P} = \pi\frac{1}{\tau_{\sigma l}^{P}}\left(1 - \frac{\tau_{\varepsilon l}^{P}}{\tau_{\sigma l}^{P}}\right)e^{-t/\tau_{\sigma l}^{P}}\theta\left(t\right) * \left(\frac{\partial v_x}{\partial x} + \frac{\partial v_z}{\partial z}\right). \tag{A16}$$

Similarly, we conduct time differentiation for the four memory variables and obtain

$$\dot{r}_{l}^{P} = -\frac{1}{\tau_{\sigma l}^{P}}\left[r_{l}^{P} + \pi\left(\frac{\tau_{\varepsilon l}^{P}}{\tau_{\sigma l}^{P}} - 1\right)\left(\frac{\partial v_x}{\partial x} + \frac{\partial v_z}{\partial z}\right)\right], \tag{A17}$$

$$\dot{r}_{xxl}^{S} = -\frac{1}{\tau_{\sigma l}^{S}}\left[r_{xxl}^{S} - 2\mu\left(\frac{\tau_{\varepsilon l}^{S}}{\tau_{\sigma l}^{S}} - 1\right)\frac{\partial v_x}{\partial x}\right], \tag{A18}$$

$$\dot{r}_{zzl}^{S} = -\frac{1}{\tau_{\sigma l}^{S}}\left[r_{zzl}^{S} - 2\mu\left(\frac{\tau_{\varepsilon l}^{S}}{\tau_{\sigma l}^{S}} - 1\right)\frac{\partial v_z}{\partial z}\right], \tag{A19}$$

$$\dot{r}_{xzl}^{S} = -\frac{1}{\tau_{\sigma l}^{S}}\left[r_{xzl}^{S} + \mu\left(\frac{\tau_{\varepsilon l}^{S}}{\tau_{\sigma l}^{S}} - 1\right)\left(\frac{\partial v_z}{\partial x} + \frac{\partial v_x}{\partial z}\right)\right]. \tag{A20}$$

Following Robertsson *et al.* (1994), the velocity–stress formulation of the viscoelastic wave equations can be derived from the constitutive relationship and the momentum conservation equation. In 2-D, with L as the number of standard linear solids, the viscoelastic wave equations are

$$\rho\dot{v}_x = \frac{\partial\sigma_{xx}}{\partial x} + \frac{\partial\sigma_{xz}}{\partial x} + f_x \tag{A21}$$

$$\rho\dot{v}_z = \frac{\partial\sigma_{xz}}{\partial z} + \frac{\partial\sigma_{zz}}{\partial z} + f_z \tag{A22}$$

$$\dot{\sigma}_{xx} = \pi S_{L}^{P}\left(\frac{\partial v_x}{\partial x} + \frac{\partial v_z}{\partial z}\right) - 2\mu S_{L}^{S}\frac{\partial v_z}{\partial z} + T^{P} + T_{xx}^{S}, \tag{A23}$$

$$\dot{\sigma}_{zz} = \pi S_{L}^{P}\left(\frac{\partial v_x}{\partial x} + \frac{\partial v_z}{\partial z}\right) - 2\mu S_{L}^{S}\frac{\partial v_x}{\partial x} + T^{P} + T_{zz}^{S}, \tag{A24}$$

$$\dot{\sigma}_{xz} = \mu S_{L}^{S}\left(\frac{\partial v_z}{\partial x} + \frac{\partial v_x}{\partial z}\right) + T_{xz}^{S}, \tag{A25}$$

where

$$S_L^P = 1 - \sum_{l=1}^{L} \left(1 - \frac{\tau_{\varepsilon l}^P}{\tau_{\sigma l}^P}\right), \tag{A26}$$

$$S_L^S = 1 - \sum_{l=1}^{L} \left(1 - \frac{\tau_{\varepsilon l}^S}{\tau_{\sigma l}^S}\right), \tag{A27}$$

$$T^P = \sum_{l=1}^{L} r_l^P, \tag{A28}$$

$$T_{zz}^P = \sum_{l=1}^{L} r_{zzl}^P, \tag{A29}$$

$$T_{zz}^S = \sum_{l=1}^{L} r_{zzl}^S, \tag{A30}$$

$$T_{xz}^S = \sum_{l=1}^{L} r_{xzl}^S, \tag{A31}$$

and where r_{ijl}^P and r_{ijl}^S are the memory variables, which can be described as

$$\dot{r}_l^P = -\frac{1}{\tau_{\sigma l}^P}\left[r_l^P + \pi\left(\frac{\tau_{\varepsilon l}^P}{\tau_{\sigma l}^P} - 1\right)\left(\frac{\partial v_x}{\partial x} + \frac{\partial v_z}{\partial z}\right)\right], \tag{A32}$$

$$\dot{r}_{xxl}^S = -\frac{1}{\tau_{\sigma l}^S}\left[r_{xxl}^S - 2\mu\left(\frac{\tau_{\varepsilon l}^S}{\tau_{\sigma l}^S} - 1\right)\frac{\partial v_x}{\partial x}\right], \tag{A33}$$

$$\dot{r}_{zzl}^S = -\frac{1}{\tau_{\sigma l}^S}\left[r_{zzl}^S - 2\mu\left(\frac{\tau_{\varepsilon l}^S}{\tau_{\sigma l}^S} - 1\right)\frac{\partial v_z}{\partial z}\right], \tag{A34}$$

$$\dot{r}_{xzl}^S = -\frac{1}{\tau_{\sigma l}^S}\left[r_{xzl}^S + \mu\left(\frac{\tau_{\varepsilon l}^S}{\tau_{\sigma l}^S} - 1\right)\left(\frac{\partial v_z}{\partial x} + \frac{\partial v_x}{\partial z}\right)\right]. \tag{A35}$$

Eqs (A21)–(A25) and (A32)–(A35) form the wave propagation equations of the viscoelastic media.

APPENDIX B: DISPERSION FORMULA

The complex phase velocity of a viscoelastic model can be expressed as

$$c(\omega) = \sqrt{\frac{M(\omega)}{\rho}}. \tag{B1}$$

Substituting the complex modulus $M(\omega)$, which can be obtained from eqs (2) and (3), into the above equation, we obtain

$$c(\omega) = c_r \sqrt{\left(1 - L + \sum_{l=1}^{L} \frac{1 + i\omega\tau_{\varepsilon l}}{1 + i\omega\tau_{\sigma l}}\right)}, \tag{B2}$$

where $c_r = \sqrt{\frac{M_R}{\rho}}$ is the relaxed velocity of the medium.

According to the definition of the complex wavenumber $k(\omega) = \frac{\omega}{c(\omega)}$ and $k(\omega) = \kappa(\omega) - i \cdot \alpha(\omega)$, where $\kappa(\omega) = \mathrm{Re}[k(\omega)]$ is the real wavenumber and $\alpha(\omega) = -\mathrm{Im}[k(\omega)]$ is the attenuation factor (Aki & Richards 1980). We derive the expression of the relevant dispersion variables of the GSLS viscoelastic model.

The phase velocity can be expressed as (Aki & Richards 1980)

$$c_p(\omega) = \frac{\omega}{\kappa(\omega)}. \tag{B3}$$

Substituting eq. (B1) into eq. (B2), we obtain the following expression of the phase velocity:

$$c_p(\omega) = \frac{1}{\mathrm{Re}\left[1/c(\omega)\right]} = \frac{{c_R}^2(\omega) + {c_I}^2(\omega)}{c_R(\omega)}, \tag{B4}$$

where $c_R(\omega)$ and $c_I(\omega)$ are the real and imaginary parts of the complex velocity $c(\omega)$, respectively.

The definition of the group velocity is (Aki & Richards 1980)

$$c_g(\omega) = \frac{d\omega}{d\kappa(\omega)}. \tag{B5}$$

Substituting eq. (B1) into eq. (B4), we obtain the following expression of the group velocity

$$c_g(\omega) = \left(\frac{d\kappa(\omega)}{d\omega}\right)^{-1} = \left(\mathrm{Re}\left[\frac{d\left(\frac{\omega}{c(\omega)}\right)}{d\omega}\right]\right)^{-1}$$

$$= \left(\mathrm{Re}\left[\frac{c(\omega) - \omega \cdot \frac{dc(\omega)}{d\omega}}{c(\omega)^2}\right]\right)^{-1}. \tag{B6}$$

Substituting M_R (eq. (7)) and $c(\omega)$ (eq. (B2)) into eqs (B4) and (B6), we can obtain the phase and group velocity equations related to the viscoelastic parameters.